Leaving Groups Prolong the Duration of 20S Proteasome Inhibition and Enhance the Potency of Salinosporamides

Rama Rao Manam,[†] Katherine A. McArthur,[†] Ta-Hsiang Chao,[†] Jeffrey Weiss,[†] Janid A. Ali,[‡] Vito J. Palombella,[‡] Michael Groll,[§] G. Kenneth Lloyd,[†] Michael A. Palladino,[†] Saskia T. C. Neuteboom,[†] Venkat R. Macherla,[†] and Barbara C. M. Potts*[,†]

Nereus Pharmaceuticals, Inc., 10480 Wateridge Circle, San Diego, California 92121, Infinity Pharmaceuticals, 780 Memorial Drive, Cambridge, Massachusetts 02139, and Center for Integrated Protein Science at the Department Chemie, Lehrstuhl für Biochemie, Technische Universität München, Lichtenbergstrasse 4, Garching D-85747, Germany

Received May 12, 2008

Salinosporamide A (**1** (NPI-0052)) is a potent, monochlorinated 20S proteasome inhibitor in clinical trials for the treatment of cancer. To elucidate the role of the chlorine leaving group (LG), we synthesized analogues with a range of LG potentials and determined their IC_{50} values for inhibition of chymotrypsin-like (CT-L), trypsin-like (T-L), and caspase-like (C-L) activities of 20S proteasomes. Proteasome activity was also determined before and after attempted removal of the inhibitors by dialysis. Analogues bearing substituents with good LG potential exhibited the greatest potency and prolonged duration of proteasome inhibition, with no recovery after 24 h of dialysis. In contrast, activity was restored after ≤12 h in the case of non-LG analogues. Intermediate results were observed for fluorosalinosporamide, with poor LG potential. Kinetic studies indicate that **1** acts as a classical slow, tight inhibitor of the CT-L, T-L, and C-L activities and that inhibition occurs via a two-step mechanism involving reversible recognition followed by rate-limiting formation of a covalent enzyme−inhibitor complex.

The 26S proteasome is a multicatalytic enzyme complex that is responsible for degradation of intracellular proteins, and has emerged as an important target in cancer chemotherapy.[1,2] Proteasome substrates include misfolded or aged proteins, the accumulation of which may trigger apoptosis, as well as those proteins that regulate cell proliferation and survival pathways.[1−4] Proteasome structural biology has provided an in-depth understanding of the mechanisms of substrate hydrolysis and inhibition by structurally diverse inhibitors.[5−7] The 26S proteasome comprises one or two 19S regulatory caps and a proteolytic 20S core particle in which protein degradation occurs. The 20S proteasome is constructed from 28 subunits forming four stacked rings, effectively creating a central cavity through which protein substrates enter and undergo hydrolysis and via which peptide hydrolysis products exit.[8,9] The two central rings each contain three pairs of proteolytic subunits (β5, β2, and β1) for which chymotrypsin-like (CT-L[a]), trypsin-like (T-L), and caspase-like (C-L) activities have been respectively conferred on the basis of their substrate specificities.[10] The active sites of each of these proteolytic subunits utilize the N-terminus ($Thr1NH_2$) as the catalytic residue during substrate hydrolysis.[9] Inhibition of at least one of the three types of proteolytic activities inhibits protein substrate turnover, although multisite inhibition has been shown to be more effective, and perhaps even synergistic, in decreasing proteolysis.[11] Thus, compounds that block hydrolysis at multiple sites may be more effective inhibitors of proteasome-mediated events and may therefore represent superior therapeutic agents.

The first proteasome inhibitor to offer clinical benefits to patients was bortezomib ((*R*)-3-methyl-1-((*S*)-3-phenyl-2-(pyrazine-2-carboxamido)propanamido)butylboronic acid), a peptide boronic acid that received regulatory approval in 2003 for the treatment of relapsed and relapsed/refractory multiple myeloma and in 2006 for the treatment of mantle cell lymphoma, effectively validating the proteasome as a target in oncology.[12−14] Salinosporamide A (**1** (NPI-0052))[15] and other related β-lactone-γ-lactams (e.g., omuralide (**2**),[16−18] **3**,[19] salinosporamide B (**4**), and other congeners[20−22]) represent a structurally distinct class of 20S proteasome inhibitors, with **1** in clinical trials for the treatment of various cancers.[15,23−25] One of the distinguishing structural features of the marine-derived inhibitor **1** is the chloroethyl group, which imparts enhanced inhibitory activity against isolated proteasomes and increased cytotoxicity against tumor cell lines.[15,21] In 2006, we published the crystal structure of **1** and its deschloro analogue **4** in complex with the yeast 20S proteasome and demonstrated that the chlorine of **1** acts as a leaving group (LG) within the 20S proteasome active sites.[26] A survey of the literature, together with our work, indicated that each of the various β-lactone-γ-lactams exhibits unique proteasome inhibition characteristics, including their *profiles* of inhibition against the three 20S proteolytic subunits and, interestingly, the apparent *duration* of their inhibition.[19,21,23,27] Thus, we considered the crystal structures of the bound forms of **1**, **2**, and **4** in light of these reported data and hypothesized that the chlorine elimination reaction (Scheme 1) renders **1** "irreversibly bound" to the proteasome. Our rationale was based on the observation that for all three compounds, the crystal structure of the complex indicates that the catalytic N-terminal

* To whom correspondence should be addressed. Phone: 858-200-8324. Fax: 858-200-8356. E-mail: bpotts@nereuspharm.com.

[†] Nereus Pharmaceuticals, Inc.

[‡] Infinity Pharmaceuticals.

[§] Technische Universität München.

[a] Abbreviations: LG, leaving group; CT-L, chymotrypsin-like; T-L, trypsin-like; C-L, caspase-like; NUK, nucleophilic water; ADME, absorption, distribution, metabolism, and excretion; TBAF, tetrabutylammonium fluoride; DAST, (diethylamino)sulfur trifluoride; AMC, 7-amino-4-methylcoumarin; IC_{50}, concentration that results in 50% inhibition; EI, enzyme−inhibitor complex; ACN, acetonitrile; TFA, trifluoroacetic acid; SDS, sodium dodecyl sulfate; HEPES, 4-(2-hydroxyethyl)piperazine-1-ethanesulfonic acid; Suc-LLVY-AMC, succinyl-Leu-Leu-Val-Tyr-7-amino-4-methylcoumarin; *Z*-LLE-AMC, *Z*-Leu-Leu-Glu-7-amino-4-methylcoumarin; Bz-VGR-AMC, Bz-Val-Gly-Arg-7-amino-4-methylcoumarin; EDTA, ethylenediaminetetraacetic acid; PDA, photodiode array.

10.1021/jm800548b CCC: $40.75
Published on Web 10/22/2008

Scheme 1. Mechanisms of Inhibition of the 20S Proteasome by (a) Leaving Groups (LG) and (b) Nonleaving Group (NLG) Analogues and Potential Pathways for Recovery of Enzymatic Activity and Competing Aqueous Hydrolysis[a]

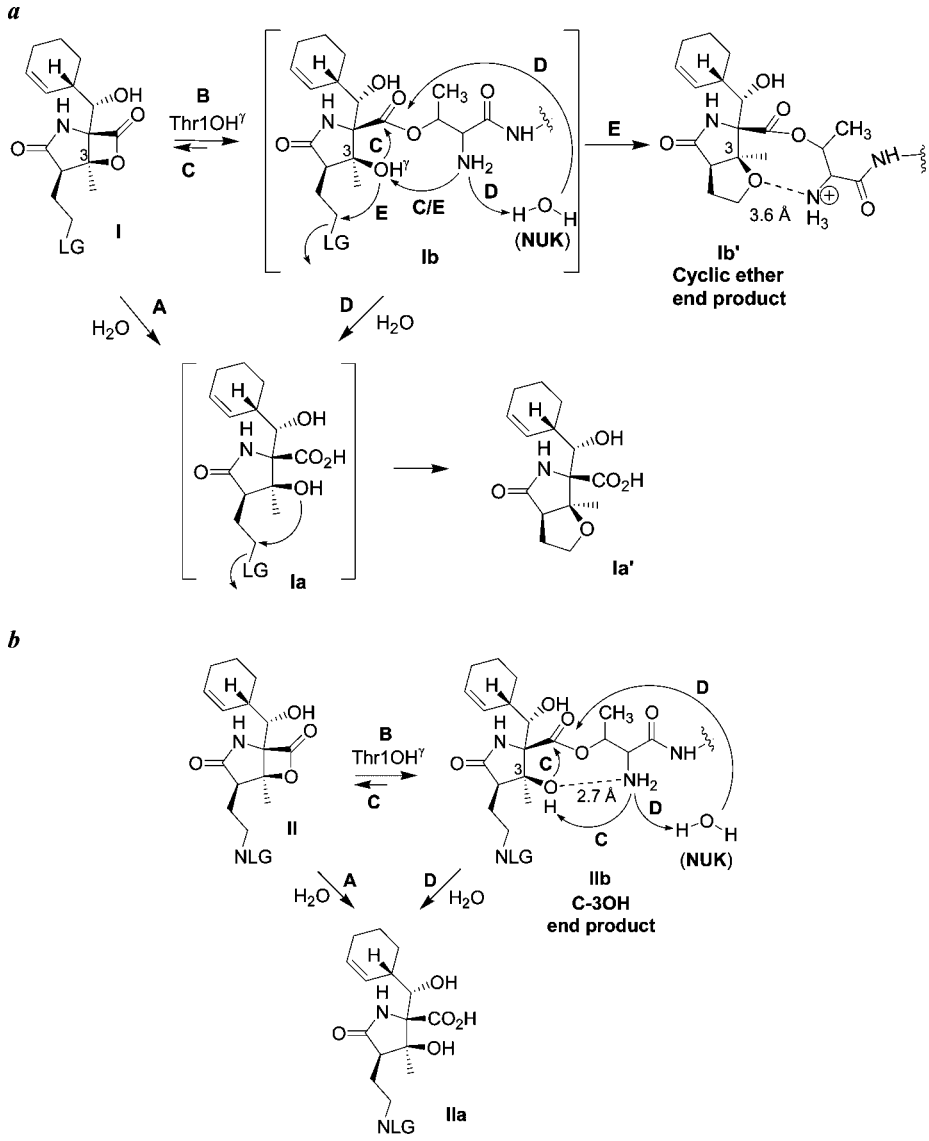

[a] (A) Aqueous hydrolysis of β-lactone in solution; (B) ester formation between the inhibitor and Thr1O$^{\gamma}$; (C) re-formation of the β-lactone within the proteasome active site; (D) hydrolysis of the inhibitor−Thr1O$^{\gamma}$ ester bond; (E) intramolecular nucleophilic displacement of the LG. In the case of **1** (LG = Cl) and **4** (NLG = H), the distances between the C-3O and Thr1N are 2.7 (**IIb**) and 3.6 Å (**Ib′**), respectively, in the crystal structure with the yeast 20S proteasome (dashed lines).[26]

Thr1O$^{\gamma}$ reacts with the β-lactone to form a covalent ester linkage between the inhibitor and the enzyme active site, but the unique presence of the chlorine LG in the case of **1** results in its subsequent elimination to give rise to a cyclic ether end product (**Ib′**, Scheme 1). We further noted that after the β-lactone ring of **2** or **4** is cleaved, C-3OH occupies the position formerly assumed by a well-defined and mechanistically important water molecule ("NUK") in the unligated form. In **1**, C-3O is similarly situated, albeit within the cyclic ether ring system. This led us to hypothesize that by blocking access to nucleophilic water, C-3O could interfere with deacylation of Thr1O$^{\gamma}$, thereby preventing or attenuating the rate of hydrolysis of the inhibitor from the protein (i.e., rendering the inhibitor a poor substrate for hydrolysis by the enzyme).[26] However, this would hold true for all of the β-lactone inhibitors under consideration. We also recognized that our hypothesis was based on static crystal structures and a body of data on the duration of proteasome inhibition drawn from distinct molecules under diverse conditions. For example, proteasome inhibition profiles in packed whole blood after iv administration of **3**[19] or **1**[23] were reported on the basis of studies in humans and mice, respectively, thus reflecting different carbon skeletons (i.e., "omuralide" versus "salinosporamide" backbones) administered to different species and evaluated by different investigators at different times, and further distinguished by various pharmacokinetic and ADME properties of each compound in vivo. The data indicated that proteasome inhibition by **3** recovered more quickly (within 24 h)[19] than that of **1** (>72 h).[23] In contrast, lactacystin (Chart 1),[16] the thioester natural product precursor of omuralide (**2**)[18] and the "model" for the synthetic **3**,[19] was reported to irreversibly inhibit the CT-L and T-L sites under conditions of serial dilution and ultrafiltration.[27] These reports created challenges in our effort to understand the relative duration of inhibition. In order to substantiate our hypothesis that halogen elimination imparts extended duration of inhibition or "irreversible binding" of **1**,[26] a systematic study was undertaken. We designed and synthesized a series of analogues such that we could directly compare congeners bearing substituents representing a range

Chart 1

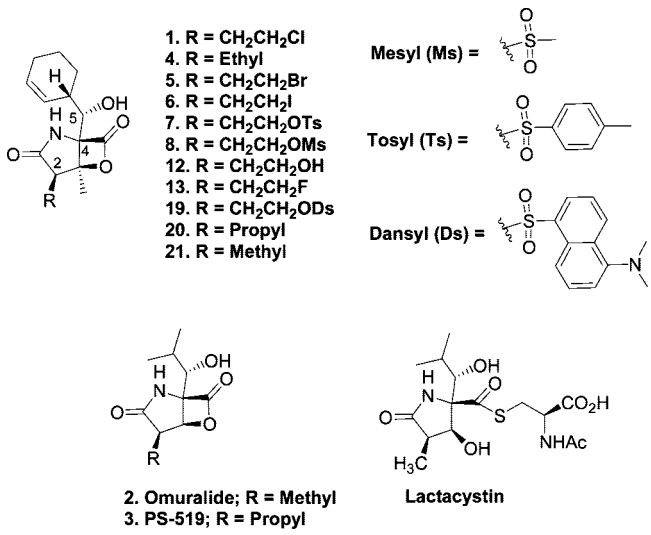

of LG potentials, including halogen LGs, non-halogen LGs, and non-LGs, with all other structural features being essentially the same (i.e., within the "salinosporamide" carbon skeleton). This series was evaluated for chemical stability and activity against isolated rabbit 20S proteasomes in vitro to establish their inhibition profiles with respect to the three 20S proteolytic functions. Since determining a kinetic off-rate for a covalent, "irreversible" inhibitor is, by definition, impractical, a qualitative evaluation of the relative duration of proteasome inhibition was performed over time under conditions of dialysis for the various proteasome−inhibitor complexes. Finally, proteasome inhibition kinetics are presented for **1** with respect to the CT-L, T-L, and C-L binding sites, and the relative inhibition profiles for the analogues are considered in the context of these findings. The proteasome inhibition profiles for **1** and **4** were also established against yeast 20S proteasomes to support correlations between the crystal structure data (determined using yeast 20S)[26] and the inhibition and kinetics data (determined using rabbit and human 20S proteasomes).

Results

Synthesis and Chemical Stability of Inhibitors. We previously reported SAR studies on **1**, which demonstrated that replacement of the chloroethyl group with unhalogenated substituents resulted in reduced potency for both 20S proteasome inhibition and cytotoxicity, while replacement of chlorine with bromine (**5**) or iodine (**6**) resulted in equipotent analogues.[21] These data clearly indicated that the halogen contributes to the potency of this class of proteasome inhibitor. As this trend could be associated with the LG property and/or its identity as a halogen, we decided to prepare analogues in which the chlorine is replaced with a non-halogen LG or a poor LG halogen (i.e., fluorine). We rationalized that various LGs, including sterically demanding ones, could be accommodated within the binding site given that the crystal structure of **4** in complex with the 20S proteasome core particle showed that the side chain bearing the LG (R, Chart 1) is pointing to the open cavity associated with the "S2" binding pocket.[26] Initially, we targeted the synthesis of the tosyl (**7**) and mesyl (**8**) analogues. Our recent report on the enantioaselective total synthesis of (−)-**1** from D-serine[28] provided an intermediate with a hydroxyethyl group (**9**) that could be derivatized with the appropriate LG and converted to the final target compound after subsequent epimerization of C-5 (Scheme 2). Treatment of **9** with tosyl chloride

Scheme 2. Total Synthesis of Tosyl Derivative (**7**) from **9**[28,a]

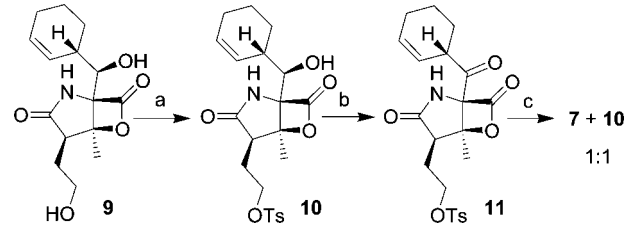

[a] (a) TsCl, Et_3N, CH_2Cl_2, room temp, 7 h, 66%; (b) Dess−Martin periodinane, CH_2Cl_2, room temp, 4 h, 75%; (c) $NaBH_4$, IPA, 1% H_2O, room temp, 5 min, 80%.

Scheme 3. Synthesis of Tosyl (**7**), Mesyl (**8**) and Dansyl (**19**) Derivatives[a]

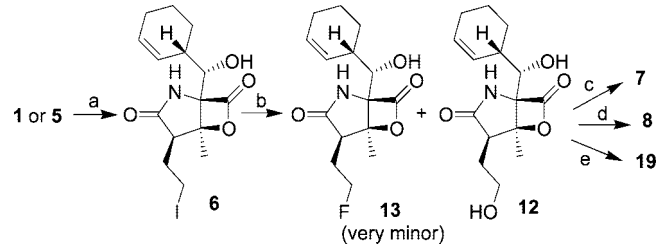

[a] (a) NaI, acetone, 6 days, 11% from **1**; NaI, acetone, 2 days, 84% from **5**; (b) AgF, THF, room temp, 16 h, 15% of **12**; (c) TsCl, Et_3N, CH_2Cl_2, room temp; 16 h, 33%; (d) MsCl, Et_3N, CH_2Cl_2, room temp, 6 h, 40%; (e) dansyl-Cl, room temp, 1.5 days, 55%.

Scheme 4. Reaction of Compounds **9** and **15** with DAST

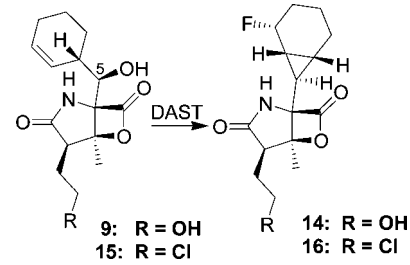

in the presence of triethylamine provided **10** selectively. In order to invert the C-5 stereocenter, **10** was oxidized with Dess−Martin periodinane, and the resulting ketone **11** was subsequently reduced with $NaBH_4$, which yielded a 1:1 mixture of diastereomers **10** and **7**.

In a parallel effort, we identified a semisynthetic method to generate hydroxysalinosporamide A (**12**) from iodosalinosporamide (**6**), which was in turn derived from **1**,[21] or more efficiently from bromosalinosporamide (**5**),[21,22,29] via halogen exchange with NaI (Scheme 3). Surprisingly, treatment of **6** with silver fluoride in an attempt to synthesize fluorosalinosporamide **13** instead produced hydroxysalinosporamide A as the major product (**12**), with **13** as a very minor byproduct. Thus, silver fluoride, which usually converts iodo to fluoro, instead gave rise to the hydroxy group in good yield. Iodo to hydroxy conversion has previously been reported using $AgNO_3$ or F_3CCO_2Ag on other small molecules.[30,31] Here, we report the use of AgF for this same conversion. This transformation provided a robust method for generation of **12**, which was previously generated in very low yield by treatment of **6** with NaOH.[21] With compound **12** in hand, treatment with tosyl or mesyl chloride in the presence of triethylamine gave the target derivatives **7** and **8**, respectively.

Alternative efforts to synthesize fluorosalinosporamide (**13**) were unsuccessful. Specifically, a direct halogen exchange

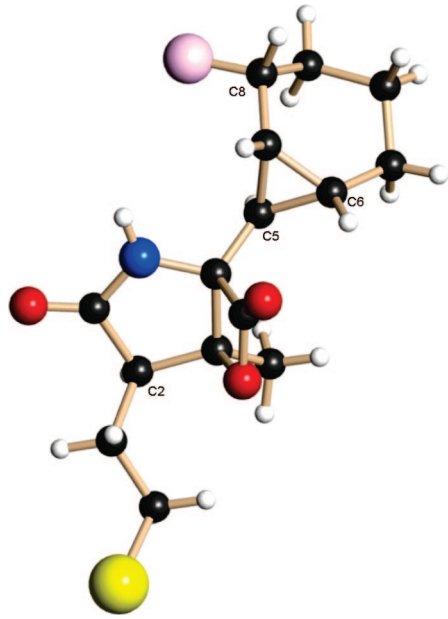

Figure 1. ORTEP figure of **16** with absolute stereochemistry established.

Scheme 5. Reaction of Compounds **1** and **12** with DAST

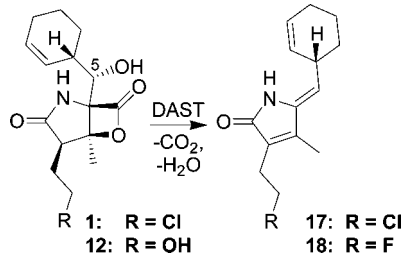

approach was attempted on **1** and **6** with halogen salts KF, NaF, and CsF and with tetrabutylammonium fluoride (TBAF) under a variety of conditions; however, no fluorinated products were observed, and the starting materials degraded under most conditions. Nucleophilic fluorinating reagent (diethylamino)sulfur trifluoride (DAST) was also used on various synthetic intermediates containing either a primary or a secondary alcohol. For example, compound **9** was reacted with DAST (Scheme 4), and while the mass spectral data for the product (**14**) were consistent with replacement of a hydroxyl group with fluorine, the proton NMR spectrum indicated that the primary alcohol was still present, but the secondary alcohol at C-5 was no longer observed. To further investigate this transformation, identical reaction conditions were used on **15**, the C-5 epimer of **1**, which gave an analogous product (**16**), for which the structure was determined by X-ray crystallography (Figure 1). Retroanalysis of the 1D NMR spectrum for **14** indicated that this fluorinated product was analogous to that of **16**, with a primary alcohol replacing C-l on the ethyl side chain. The formation of **14** and **16** can be rationalized through a homoallylcyclopropylcarbinyl rearrangement and was unique to compounds of C-5 (*R*) stereochemistry. In fact, treatment of **1** and **12** (C-5 (*S*)) with DAST gave degradants **17** and **18**, respectively (Scheme 5).[32] Thus, despite considerable efforts, very small quantities of the target fluorosalinosporamide (**13**) were obtained only after repeated rounds of purification of product obtained after treatment of **6** with AgF (Scheme 3, vide supra). Incidentally, cyclopropanyl compound **16** was only weakly active (IC_{50} > 6 μM for inhibition of rabbit 20S proteasome CT-L activity).

With mesyl and tosyl analogues in hand, we considered the potential value of incorporating a fluorescent LG that might provide a sensitive tag for monitoring the elimination of the LG under a variety of assay conditions. Previous reports indicated that dansyl has been effectively used in place of tosyl.[33] Thus, dansyl analogue **19** was synthesized using the analogous process described above for **7** and **8**.

With the target analogues in hand, the stability of each compound was evaluated in the proteasome assay buffer with the following goals: (i) to assess the stability of the β-lactone ring, which is required to react with Thr1O$^{\gamma}$ in the first step of the proteasome inhibition reaction sequence (vide infra); (ii) to determine whether stability correlates with potency; and (iii) to confirm LG potential. The kinetics and mechanism of hydrolysis of **1**, its conversion to **Ia** (Scheme 1; LG = Cl), and ultimate formation of **Ia′** were previously studied by Denora et al.,[34] who showed that loss of **1** followed pseudo-first-order kinetics. Curve fitting the loss of **1** and formation and loss of **Ia** indicated that the reaction followed the simple pathway **I** → **Ia** → **Ia′** and that β-lactone ring hydrolysis preceded chlorine elimination. Thus, the chlorine LG did not appear to directly impact the loss of **1**. These findings provided a basis for the present study, for which the kinetics appear to qualitatively follow the same pattern, where β-lactone ring hydrolysis precedes LG elimination when a LG is present.

Analogue solutions were prepared in the proteasome assay buffer (20 mM HEPES buffer, pH 7.3) at 37 °C and analyzed by LC−MS such that the disappearance of starting compound (**I** or **II**, Scheme 1) could be monitored over time (Figure 2). The $T_{1/2}$ values (Table 1) representing the loss of the intact drug were determined directly from the curves, and no curve fitting was attempted. To provide further insights into the degradation pathway for each compound, the appearance of hydrolysis product(s) (**Ia**, **Ia′**, or **IIa**) was also plotted (Figure 2). Compounds that gave rise to the cyclic ether end product **Ia′** (Scheme 1a) were classed as bearing a LG.

$T_{1/2}$ values were at least 1 h across the analogue series, which is significantly longer than the drug−proteasome preincubation time in the proteasome activity assay (5 min), indicating that chemical hydrolysis of starting compound was minimal and thus has little to no impact on the potency measurement. Moreover, there was no apparent correlation between $T_{1/2}$ and the IC_{50} values in proteasome inhibition assays (Table 1) and no definitive difference in stability to distinguish the LG and non-LG classes. In fact, the most stable compounds in the series ($T_{1/2}$ > 2.5 h) were represented by members of both the LG (dansyl (**19**)) and non-LG (ethyl (**4**) and propyl (**20**)) classes.

For LG analogues, β-lactone ring hydrolysis is followed by LG elimination. The transient intermediate product of β-lactone hydrolysis (**Ia**) was observed only in the cases of **1** and fluorosalinosporamide (**13**) (Figure 2). This finding is consistent with the relative LG potential of the analogues in this series, where the transformation of **Ia** to **Ia′** is apparently very rapid for the tosyl, dansyl, iodo, mesyl, and bromo analogues, intermediate for the parent chlorinated compound (**1**), and very slow for fluorosalinosporamide (**13**), which bears the poorest LG. Complete conversion of the β-lactone hydrolysis product of **13** to the cyclic ether end product was slow but steady over 5 days (Figure 2e). Intramolecular displacement of fluoride to form cyclic ethers has been reported previously.[35,36]

Proteasome Inhibition Profiles for LG and Non-LG Analogues. Non-halogen LG analogues **7**, **8**, and **19** were evaluated for inhibition of the CT-L, T-L, and C-L activities of isolated rabbit 20S proteasomes and compared to those of non-

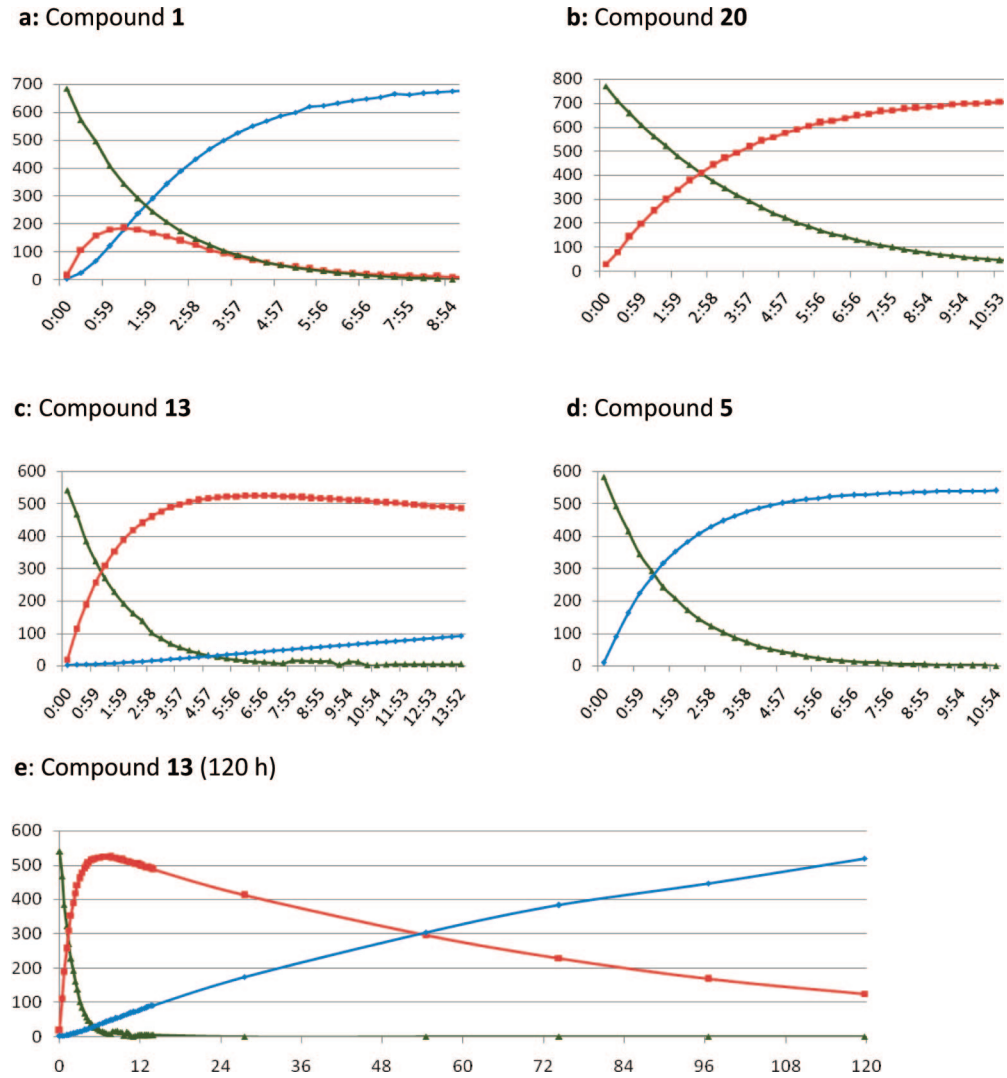

Figure 2. Hydrolysis of **1**, **5**, **13**, and **20** over time in proteasome assay buffer at pH 7.3 and 37 °C. Green (▲), red (■), and blue (●) lines represent starting material (**I** or **II**), β-lactone ring hydrolysis product (**Ia** or **IIa**), and cyclic ether (**Ia′**), respectively (see Scheme 1). *X*-axis is time in hours and minutes. *Y*-axis is UV peak area in mAU·s: (a) hydrolysis of **1**; (b) hydrolysis of **20** (similar patterns of hydrolysis products were observed for **4**, **12**, and **21**); (c) hydrolysis of **13**; (d) hydrolysis of **5** (similar patterns of hydrolysis products were observed for **6**, **7**, **8**, and **19**).

LG and halogen LG analogues (Table 1). Because of limited quantities of **13**, only inhibition of CT-L activity was evaluated. In general, analogues bearing substituents with good leaving potential were more potent inhibitors of all three proteolytic subunits compared to non-LG analogues. All of the analogues were potent inhibitors of the rabbit 20S proteasome CT-L activity, with IC_{50} values ranging from 2.5 to 4.3 nM for LG analogues, 10 nM for fluorosalinosporamide, with weak LG potential, and from 7.5 to 26 nM for non-LG analogues. With respect to inhibition of T-L activity, IC_{50} values ranged from 10 to 65 nM for LG analogues and from 370 to 1200 nM for non-LG analogues. Notably, the tosyl (**7**) and dansyl (**19**) analogues were highly potent inhibitors of *all three* proteolytic activities. A recent report on the impact of inhibition of multiple proteolytic subunits[11] suggests that these compounds should be extremely effective inhibitors of protein degradation. The low IC_{50} values for **7** and **19** demonstrate that the steric bulk of aromatic sulfonate ester substituents is well accommodated within all three ligand binding sites (prior to elimination). This finding is consistent with the open cavity associated with the "S2" binding pocket of the proteolytic subunits[8] and also indicative of enhanced binding energetics with respect to the T-L and C-L sites. The low IC_{50} values for the iodo (**6**) and bromo (**5**) analogues with respect to the T-L site further demonstrated the affinity of analogues bearing larger substituents for this subunit. Prior to this report, the largest side chain described for analogues in this family was *n*-hexyl or 2-OH-*n*-hexyl.[37]

We also evaluated **1** and **4** for inhibition of yeast 20S proteasomes. IC_{50} values of each compound for the CT-L, T-L, and C-L sites followed the same trends observed for rabbit and human 20S proteasomes (Table 1), thereby establishing a basis for correlating the crystal structure data obtained with yeast 20S proteasomes[26] with the inhibition and kinetics data obtained using rabbit and human 20S proteasomes discussed herein.

Inhibition/Recovery of 20S Proteasome−Inhibitor Complexes. A qualitative assessment of the relative duration of proteasome inhibition by analogues in the LG versus non-LG classes was made by evaluation of 20S proteasome activity after dialysis. For evaluation of CT-L activity, we selected **1** along with the most potent (tosyl, **7**) and least potent (mesyl, **8**) compounds within the LG class, plus fluorosalinosporamide (**13**), with poor LG potential. For non-LG analogues, we evaluated the methyl (**21**), ethyl (**4**), propyl (**20**), and hydroxyl (**12**) analogues. Rabbit 20S proteasomes were pretreated for 1 h with the representative analogues at their respective IC_{50} values,

Table 1. Inhibition of the CT-L, T-L, and C-L Activities of 20S Proteasomes from Rabbit (unless Otherwise Indicated) and β-Lactone Hydrolysis Rates ($T_{1/2}$) for **1** and Analogues

compd	R	leaving group	$T_{1/2}$ (min)	IC_{50} (nM)[a] CT-L	T-L	C-L
1[e]	CH_2CH_2Cl	yes	77 ± 5	2.0 ± 0.3[b]	59 ± 1[b]	2600 ± 200[b]
				3.5 ± 0.3[c]	28 ± 2[c]	430 ± 34[c]
				2.5 ± 1.2	26 ± 2	330 ± 25
6	CH_2CH_2I	yes	92	2.8 ± 0.5[d]	13 ± 3[d]	410 ± 230[d]
5	CH_2CH_2Br	yes	80	2.6 ± 0.4[d]	14 ± 2[d]	290 ± 60[d]
7	CH_2CH_2OTs	yes	75	2.5 ± 0.4	9.9 ± 0.2	127 ± 5
8	CH_2CH_2OMs	yes	59	4.3 ± 0.8	65 ± 8	870 ± 32
19	CH_2CH_2ODs	yes	179	3.0 ± 0.5	12 ± 2.3	90 ± 11
13	CH_2CH_2F	yes[f]	79	9.2 ± 10.2	ND	ND
12	CH_2CH_2OH	no	85	14 ± 1.5	1200 ± 150	1200 ± 57
21[e]	CH_3	no	95	7.5 ± 0.6	370 ± 44	460 ± 49
4[e]	CH_2CH_3	no	190	26 ± 6.7	610 ± 35	1200 ± 110
				16 ± 4[b]	1040 ± 140[b]	>20,000[b]
20	$CH_2CH_2CH_3$	no	171	24 ± 5[d]	1100 ± 200[d]	1200 ± 200[d]

[a] IC_{50} values represent the mean ± standard deviation of three or more experiments except for compound **13** (results of two independent experiments). ND: not determined. [b] Yeast 20S proteasomes. [c] Human 20S proteasomes, reported previously.[23] [d] Reported previously.[21] [e] Prepared as described previously.[21] [f] Very slow elimination was observed in aqueous buffer (Figure 2).

and CT-L was measured before and after attempted removal of the ligand by dialysis at room temperature over time (Figure 3a). Analogues with good LG potential inhibited CT-L activity with no appreciable recovery after 24 h of dialysis. In contrast, activity was partially recovered after 5 h and essentially restored after 12 h dialysis in the case of non-LG analogues. Interestingly, the poor LG analogue fluorosalinosporamide showed partial recovery of activity after 5 h dialysis; however, proteasome activity did not fully recover, even after 24 h of dialysis. We then evaluated **1** and **4** for recovery of T-L and C-L activities and compared the results to those obtained for the CT-L site (Figure 3b). The trend was similar for all three proteolytic sites: in the case of **1**, there was no recovery of activity after 24 h of dialysis, while activity was partially restored after 5 h and completely restored after 12 h of dialysis in the case of non-LG analogue **4**.

In an independent experiment using human 20S proteasomes, against which **1** shows an inhibition profile similar to that of both rabbit and yeast 20S proteasomes (Table 1), we evaluated the reversibility of inhibition by **1** by measuring CT-L, T-L, and C-L activity before and after attempted removal of the ligand by dialysis at room temperature. As in the case of the rabbit 20S proteasomes, **1** completely inhibited all three proteolytic sites with no recovery of enzyme activity after 12 h of dialysis.

The collective data indicate that all of the salinosporamides have very slow enzyme off-rates and that the presence of a LG dramatically prolongs the duration of inhibition. These data strongly suggest that analogues bearing substituents with good LG potential have the same end product structure in the proteasome active site as observed in the crystal structure of **1** in complex with the 20S proteasome (**Ib′**, Scheme 1).[26]

There are several possible explanations for the longer duration of proteasome inhibition exhibited by the LG analogues that have been considered previously in the context of **1** and **4**,[26] including (i) modified charge distribution and/or hydrogen bonding networks as a result of the "cyclic ether end product" versus "C-3OH" forms of the bound ligands from the LG and non-LG families, respectively (formulas **Ib′** and **IIb**, respectively; Scheme 1), and (ii) the potential for reclosure of the β-lactone ring in the case of the non-LG analogues, which would effectively hydrolyze the ligand−Thr1O$^{\gamma}$ ester bond and free the ligand (Scheme 1b, pathway C).[38] These pathways are considered in detail in the Discussion.

Proteasome Inhibition Kinetics for 1. While the dialysis experiments (vide supra) and the crystal structure of **1** in complex with the 20S proteasome[26] established **1** as a covalent and "irreversible" proteasome inhibitor, we undertook a formal evaluation of proteasome inhibition kinetics using human 20S proteasomes. To delineate the kinetic steps involved in the inhibition mechanism of **1**, we measured the hydrolysis of fluorogenic 7-amino-4-methylcoumarin (AMC) tagged) peptides specific for the three respective proteolytic sites in the presence of increasing concentrations of **1**. Peptide substrate hydrolysis was followed in a continuous manner and monitored by the release of free AMC, resulting in a concomitant increase in fluorescence (Figure 4a,c,e). In the absence of inhibitor, this increase in fluorescence was linear for 1200, 1500, and 800s for the β5 (CT-L), β2 (T-L), and β1 (C-L) sites, respectively. The presence of **1** did not result in immediate inhibition. Instead, we observed a slow onset of inhibition, resulting in a nonlinear progress curve, which became more pronounced as the concentration of **1** was increased. This is typical of slow tight binding inhibitors and is indicative of a multistep inhibition mechanism.[40] The individual progress curves were fit to eq 1,

$$P = \left[V_s t + \frac{V_0 - V_s}{k_{obs}} (1 - e^{-k_{obs} t}) \right] + B \quad (1)$$

where k_{obs} is the observed rate constant obtained from the primary kinetic progress curves and represents the net rate constant at which the initial noninhibited steady state substrate hydrolysis rate (V_0) was converted to the final inhibited steady state (V_s). In eq 1, B represents the baseline fluorescence.

Secondary plots of the k_{obs} with respect to inhibitor concentration were hyperbolic for the β5 (CT-L) and β2 (T-L) sites (Figure 4b,d) and is a classical indication of a two-step inhibition mechanism. The secondary plots were fitted to eq 2 to yield k_{inact} and K_i parameters.

$$k_{obs} = \frac{k_{inact}[\mathbf{1}]}{[\mathbf{1}] + K_i} \quad (2)$$

The first step, denoted by K_i, is a "recognition step" reflecting the reversible binding of **1** to the proteolytic sites (i.e., formation of EI, Scheme 6). The second step is a rate limiting step, denoted by the rate constant k_{inact} and likely involves the nucleophilic attack of Thr1O$^{\gamma}$ on the β-lactone ring, resulting in a covalent enzyme−inhibitor complex (EI*).

Because the first step is reversible, we determined meaningful thermodynamically K_i parameters of 23 and 97 nM for the β5 (CT-L) and β2 (T-L) sites, respectively. We also determined the inactivation rate constants k_{inact}, the net rate constant for the formation of a covalent bond between the β-lactone and the enzyme. For the β5 (CT-L) and β2 (T-L) sites, we determined inactivation rate constants of $k_{inact} = 0.01$ and 0.003 s^{-1}, respectively. These results indicate that **1** has both a higher initial affinity (K_i) and a faster inactivation rate constant (k_{inact}) for the CT-L site compared to the T-L site.

The primary data for the C-L site were analyzed in an identical manner, but the secondary plots yielded a linear relationship between k_{obs} and [**1**] (Figure 4f). Two models were used to fit these data. The simplest is a one-step inhibition mechanism described by eq 3, where k_{on} is the second-order binding constant:

$$k_{obs} = k_{on}[\mathbf{1}] \quad (3)$$

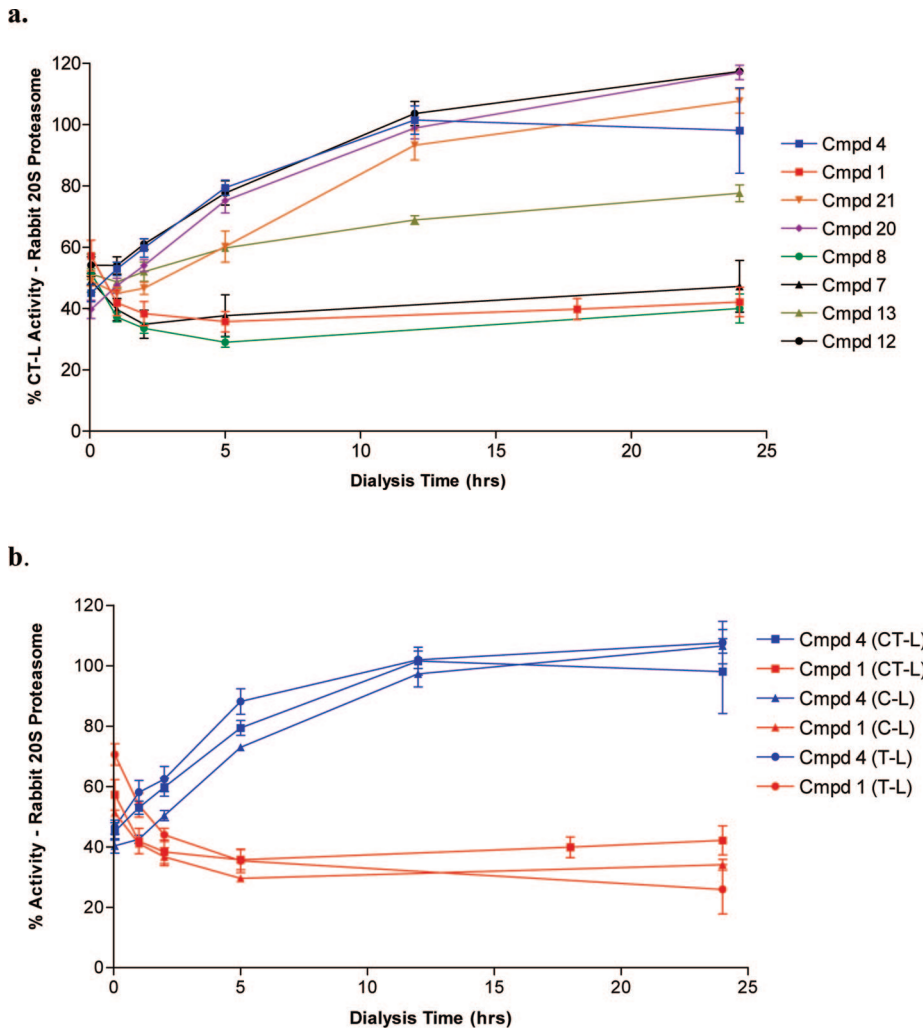

Figure 3. Recovery of 20S proteasome activity upon dialysis of proteasome−analogue complexes for the (a) CT-L after preincubation with **1**, **4**, **7**, **8**, **12**, **13**, **20**, and **21** and (b) CT-L, T-L, and C-L sites after preincubation with **1** and **4**.

This kinetic scheme would be consistent with an irreversible mechanism if the covalent bond was formed instantaneously after the initial binding step. However, the initial binding step via such a one-step binding mechanism would yield a second-order binding constant $k_{on} = 2 \times 10^4\ M^{-1}\ s^{-1}$, which is 5000 to 50000-fold slower than diffusion-controlled binding and thus unrealistic. The striking nonlinearity of the primary data with respect to increasing concentrations of **1** (Figure 4e) is more typical of a slow tight binding inhibitor and a two-step inhibition mechanism, with the second step being rate limiting, i.e., analogous to the CT-L and T-L sites but characterized by different relative rates for K_i and k_{inact}. Thus, fitting the C-L secondary plot to a two-step mechanism and eq 2 yielded an initial reversible binding K_i of $>1\ \mu M$ and an inactivation rate constant k_{inact} of $>0.02\ s^{-1}$.

The collective data (Table 2) indicate that there is initial tight reversible binding of **1** to the CT-L and T-L sites and hence good molecular recognition, which bodes well for specificity. However, the reversible binding of **1** to the C-L site is relatively weak in comparison, and the inhibition of the C-L site is driven by the irreversible nature of the nucleophilic attack on the β-lactone ring.

These findings are consistent with the relative IC_{50} values of **1** for inhibition of the three proteolytic subunits of rabbit, human, and yeast 20S proteasomes (Table 1), which indicate that the relative potency of **1** (and its analogues) for the three subunits follow the trend CT-L > T-L ≫ C-L. However, the kinetics of an irreversible inhibitor cannot be directly linked to specific IC_{50} values, which represent cumulative contributions to potency that are active throughout the incubation period of the drug with the enzyme. For an irreversible inhibitor, the IC_{50} measured at one time point will be different and weaker than that measured at a later time point because the irreversible nature of the inhibition acts as a sink, pulling the enzyme into the fully inactivated form over time. The extent of inhibition will be dependent upon the noncovalent binding and recognition step (K_i), the inactivation step (k_{inact}), and whether the inhibitor is a "slow substrate" versus a true irreversible inhibitor. These aspects are discussed in greater detail below.

Discussion

Understanding the extent of proteasome inhibition by **1** and its analogues requires consideration of the various steps associated with the enzyme inhibition process. The first step, noncovalent binding or recognition of the enzyme active site by the inhibitor, has been described by detailed kinetic analysis of **1** for the three proteolytic sites (vide supra) and demonstrates that **1** has a very high affinity for both the CT-L and T-L sites and a weaker affinity for the C-L site. The analogous trend in IC_{50} values for **1** and its analogues (Table 1) suggests that the entire family of compounds evaluated in this study follows the same trend for relative affinities for the three proteolytic sites (CT-L

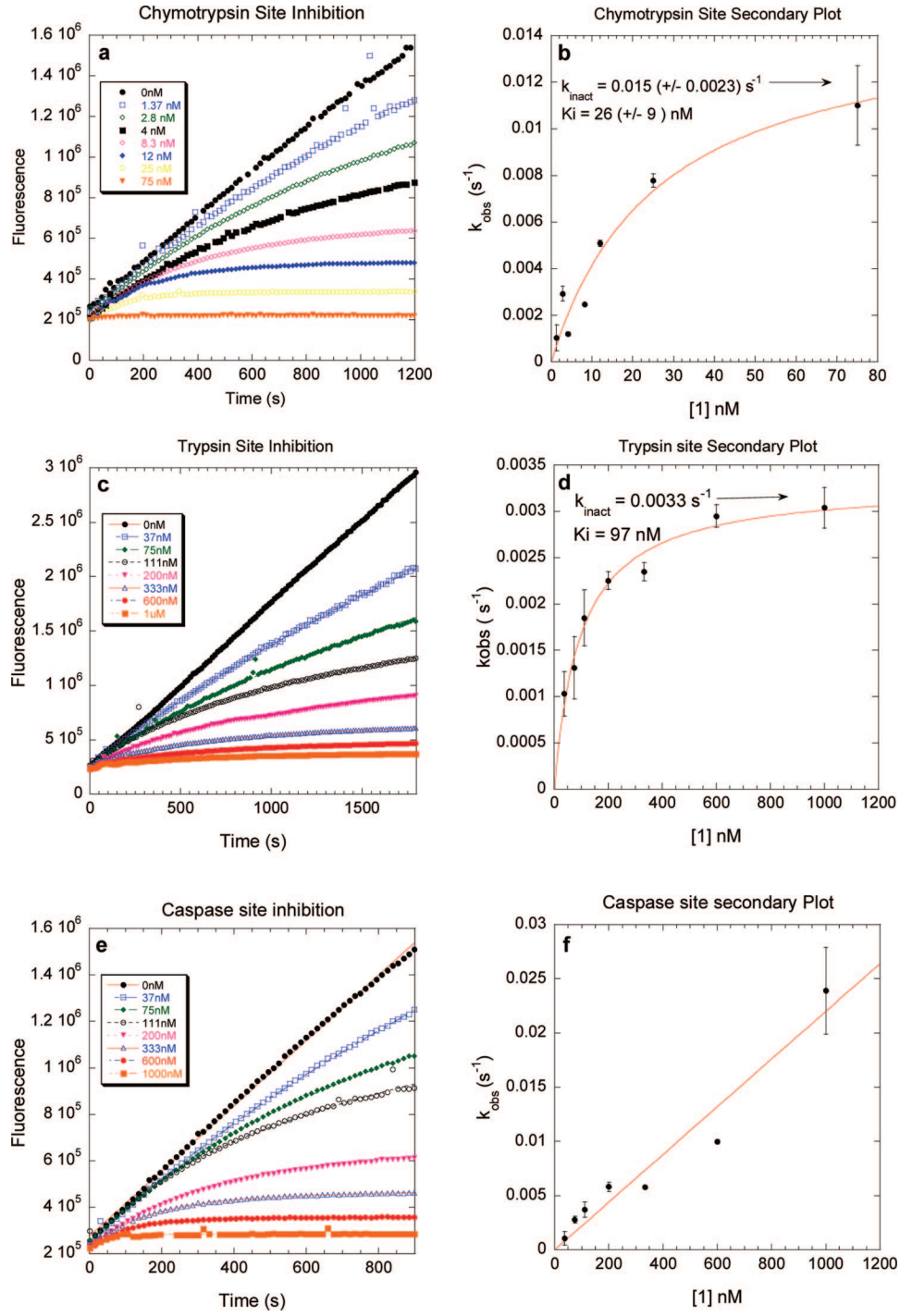

Figure 4. Inhibition kinetics for the CT-L (a, b), T-L (c, d), and C-L (e, f) sites of human 20S proteasomes by compound **1**. Peptide substrate hydrolysis was monitored by increase in fluorescence (reflecting release of free AMC substrate) over time at various concentrations of **1** (left panels). Secondary plots of k_{obs} versus inhibitor concentration (right panels) were hyperbolic for the CT-L and T-L sites and linear with respect to the C-L site.

Scheme 6

$$E + I \underset{}{\overset{K_i}{\rightleftharpoons}} EI \xrightarrow{k_{inact}} EI^*$$

> T-L ≫ C-L). The higher affinity for the CT-L site compared to the T-L site may be attributed to the more spacious S1 binding (recognition) pocket of the T-L site, which requires a greater decrease in entropy of binding. The potential for greater mobility of the inhibitor within the T-L site may result in a less stable noncovalent adduct with perhaps shorter residence time in the active site, which may in turn decrease the rate of covalent binding. Further contributions to the entropy of binding are apparent from the relative extents of inhibition by the various analogues. For example, several R groups (Chart 1) provide the potential for increased motion; consider the "wagging" of the ethyl, hydroxyethyl, and propyl side chains of **4**, **12**, and

Table 2. Dissociation Constants (K_i) and Rates of Inactivation (k_{inact}) for the $\beta5$, $\beta2$, and $\beta1$ Subunits by Compound **1**

inhibition kinetics for **1**	$\beta5$ (CT-L)	$\beta2$ (T-L)	$\beta1$ (C-L)
K_i (nM)	23	97	>1000
k_{inact} (s^{-1})	0.01	0.003	≫0.02

20 compared to the more rigid methyl group of the most potent non-LG analogue in the series, **21**. The variation in IC_{50} values among LG analogues is also suggestive of contributions from differences in their binding energetics, as the stability of the common, constrained cyclic ether end product is the same in each case and thus cannot account for the differences in IC_{50} values across the LG family.

The second step of proteasome inhibition for compounds in the salinosporamide family involves formation of a covalent ester linkage between Thr1O$^{\gamma}$ and the β-lactone ring of each of the inhibitors. In the case of the LG analogues, this step is followed by nucleophilic displacement of the LG to give rise to common cyclic ether end product. There are favorable enthalpic changes associated with LG elimination, and while the end product is more rigid, representing a decrease in entropy, the freeing of the LG contributes an increase in entropy, as previously discussed in the context of **1** and **4**.[26] We note that the rank order for the IC_{50} values among LG analogues does not *strictly* follow established trends for LG potential ($ArSO_2O^- > I^- > CH_3SO_2O^-$ (OMs) $> Br^- > Cl^- > F^-$).[41] This observation further highlights the contribution of the inhibitor's affinity for the active site to the IC_{50} value, which is further enhanced by the subsequent covalent reaction between Thr1O$^{\gamma}$ and the β-lactone of the inhibitor and ultimate displacement of the LG.

Finally, we consider the relative duration of proteasome inhibition for analogues in the LG versus non-LG subfamilies. The dialysis data (Figure 3) indicate that analogues bearing substituents with good LG potential have much longer duration of proteasome inhibition (no recovery of activity after 24 h of dialysis) than non-LG analogues (partial recovery after 5 h and complete recovery after 12 h of dialysis) for all three proteolytic subunits. This suggests that the cyclic ether end product **Ib′** derived from LG analogues is much more stable than the C-3OH end product **IIb** from the non-LG family (Scheme 1). [The unique case of **13**, bearing a poor LG and falling between the two classes, is discussed in greater detail below.] The factors responsible for the greater stability of the adducts formed between LG analogues and the 20S proteasome active site remain to be fully elucidated but may include (i) the unique charge distribution of the cyclic ether end product, i.e., full protonation of the catalytic N-terminus (Thr1NH_3^+, Scheme 1), such that it cannot catalyze hydrolysis of the inhibitor−Thr1O$^{\gamma}$ ester, (ii) exclusion of nucleophilic water (NUK), and/or (iii) inability to re-form the β-lactone ring, as discussed below. In any event, these factors are apparently equally effective in all three proteolytic subunits.

The C-3O of the end products derived from both LG and non-LG analogues is well positioned to interfere with access by nucleophilic water (NUK), thereby attenuating the rate of hydrolysis of the ester linkage between the inhibitor and Thr1O$^{\gamma}$.[26] NUK, having been displaced from its formal position in the active site upon binding of the inhibitor, must now compete with C3-OH. The rate of hydrolysis of this bond, which is required to free the inhibitor from the active site, is apparently different for analogues bearing substituents with good LG potential (no detectable hydrolysis) and non-LG (slowly hydrolyzed) inhibitors. On the basis of these dialysis data, the non-LG analogues may be kinetically described as "slow substrates" for the enzyme that can be deacylated, albeit poorly. We can hypothesize that the presence of a good LG, which enables the intramolecular cyclization reaction, prevents the deacylation reaction and effectively converts these β-lactones from "slow substrates" into true "irreversible inhibitors" that cannot undergo the deacyclation step (and hence show no recovery of activity after 24 h of dialysis).

Hydrolysis of the inhibitor−Thr1O$^{\gamma}$ ester bond requires Brownian motions and thermodynamics that favor nucleophilic water (NUK) achieving the correct position to attack the carbonyl carbon of the ester linkage. This is highly unfavorable in the case of the cyclic ether end product (**Ib′**) derived from LG analogues, for which ester hydrolysis apparently does not occur to any appreciable extent. In addition to NUK having to overcome the steric interference described above, ester hydrolysis will be attenuated so long as the N-terminus remains in the protonated state (Thr1NH_3^+). Hydrolysis by NUK (Scheme 1, pathway D) appears to be more favorable in the case of the non-LG inhibitor−enzyme adducts (**IIb**), given that recovery of enzymatic activity is ultimately recovered after dialysis. Alternatively, one might conclude that NUK is similarly excluded in both cases, which then requires that cleavage of the ester bond occurs via the *pathway available exclusively to non-LG analogues*, i.e., re-formation of the β-lactone ring (Scheme 1b, pathway C). As this pathway is not accessible to the cyclic ether end product borne from LG analogues (**Ib′**), it could certainly explain their behavior as irreversible inhibitors as opposed to slow substrates. While re-formation of the β-lactone ring might be considered energetically unfavorable, the catalytic Thr1NH_2 (which acts as a base during peptide substrate hydrolysis, abstracting a proton from NUK to catalyze hydrolysis of the substrate−Thr1O$^{\gamma}$ ester bond[5,7,8]) is well positioned to catalyze this reaction. In fact, in the crystal structure of **4** in complex with the 20S proteasome core particle, the distance between C3−O and Thr1N is 2.7 Å[26] (Scheme 1b). Moreover, β-lactone ring formation has been observed in related systems, including the conversion of lactacystin to omuralide[18] and related reactions on semisynthetic thioesters of salinosporamides.[22] Thus, an optimized environment within the proteasome active site might indeed favor re-formation of the β-lactone ring. Once re-formed, the β-lactone could undergo repeat reaction with Thr1O$^{\gamma}$ (Scheme 1, pathway B); however, there is now a competing opportunity for aqueous hydrolysis (pathway A), which would circumvent further reaction of the inhibitor with the enzyme.[42] On the basis of the dialysis results, recovery from inhibition by a non-LG analogue, whether by hydrolysis of the ester bond (via NUK, pathway D) *or* by re-formation of the β-lactone ring (via C-3OH, pathway C), occurs very slowly. Slow competition between NUK and C-3OH for cleavage of the inhibitor−Thr1O$^{\gamma}$ ester bond and between water (including NUK) and Thr1O$^{\gamma}$ for a re-formed β-lactone inhibitor must ultimately favor removal of the non-LG inhibitors from the active site to slowly restore enzymatic activity.

Flurosalinosporamide (**13**) represents a unique case of partial recovery of proteasome activity after dialysis that may be interpreted within the context of the above model. While fluoride represents a poor LG, very slow conversion of **13** to **Ia′** was observed in the proteasome assay buffer (Table 1, Figure 2). If fluoride elimination also occurs within the proteasome active site, the partial recovery of enzymatic activity after dialysis might be attributed to some fraction of the bound inhibitor in the form of **Ib′**. Specifically, if intermediate **Ib** (Scheme 1a) is relatively long-lived within the proteasome active site (compared to compound **1**, for example), there may be competition between (i) elimination of fluoride (Scheme 1, pathway E), which would render the compound "irreversibly bound", and (ii) cleavage of the inhibitor−ester bond by re-formation of the β-lactone ring (pathway C) and/or hydrolysis by water (pathway D). Such competition would result in partial recovery of proteolytic

activity (resulting from the fraction that has been hydrolyzed) and ultimately stabilization to a constant level of inhibition (representing the fraction that is irreversibly bound), consistent with our observations after dialysis (Figure 3).

Fluorosalinosporamide has recently been generated by an elegant mutasynthesis and described as a reversible proteasome inhibitor based on washout experiments in comparison with **1** and **4**.[43] Inspection of the crystal structure of **4** in complex with the yeast 20S proteasome[26] suggested potential amino acid hydrogen bonding partners for **13** (i.e., in the form of **IIb**) that may contribute to its increased activity compared to **4**.[43] There are a variety of mechanisms whereby introduction of fluorine may enhance the binding affinity of a ligand for its protein target, including lipophilic interactions, favorable dipolar contacts, and the potential to act as a "true" hydrogen-bond acceptor.[44−47] While hydrogen bonds involving organic fluorine are considered rare,[48,49] a survey of the Protein Data Bank for crystal structures of proteins cocrystallized with fluorine-containing ligands offers some examples of [R−F···H-donor] contacts.[50] Such interactions may be at play in the case of fluorosalinosporamide (**13**) but may not be sufficient to explain its enhanced duration of proteasome inhibition compared to non-LG analogues. The hydrogen bond strength for an [R−F···H-donor] contact is, at best, half that of the analogous interaction involving oxygen ([R−O···H-donor]),[44,48] and yet dialysis-induced recovery of proteasome activity was more rapid and complete in the case of hydroxysalinosporamide (**12**) compared to **13**. Preliminary analysis of crystal structures of fluorosalinosporamide in complex with yeast 20S proteasomes are indicative of slow elimination of fluoride (M. Groll, unpublished observations) and support the mechanism proposed in Scheme 1. Indeed, our observations to date are consistent with the unpredictable nature of interactions involving fluorine derivatives (so-called "flustrates").[51]

In summary, the extent of inhibition of the β-lactone−γ-lactam proteasome inhibitors is a product of binding and reactivity properties, together with relative off-rates (duration of inhibition). Detailed, comparative kinetic studies on a wide range of analogues in this nuanced family of inhibitors will be needed to establish the relative contributions of each of these steps to the potency of each compound.

Concluding Remarks

Our findings on LG and non-LG analogues of **1** indicate that proteasome inhibition is enhanced by the presence of a LG in a position that enables cyclic ether formation subsequent to β-lactone ring opening. Analogues that bear a substituent with good LG potential (Cl, Br, I, OMs, OTs, or ODs) give rise to a common, highly stable cyclic ether end product that cannot be deacylated and thus induce prolonged duration of proteasome inhibition. This "irreversible binding" holds true for all three proteolytic subunits. Our observations are consistent with the prolonged duration of proteasome inhibition observed in packed whole blood after iv administration of **1** in several species.[23,52] It is clearly possible to design analogues with properties intermediate between the LG (true "irreversible inhibitors") and non-LG ("slow substrate") analogues, as exemplified by fluorosalinosporamide, for which inhibition was only partially reversible. Such features may be useful in fine-tuning the duration of proteasome inhibition, which may have important therapeutic implications for the treatment of cancer, inflammation, and infectious diseases.

Experimental Section

General Experimental Procedures. NMR spectra were collected using a 500 MHz Bruker Avance spectrometer using an inverse probe equipped with *x*,*y*,*z*-gradients except for the ^{13}C NMR spectra, which were acquired with a broad-band observe probe. Data were acquired at 298 K in $CDCl_3$ referencing 7.24 and 77.00 ppm or DMSO-d_6 referencing 2.49 and 39.00 ppm for ^{1}H and ^{13}C NMR, respectively. The LC−MS data were obtained from an Agilent HP1100 HPLC equipped with an Agilent photodiode array (PDA) detector and MSD system. The mobile phase was a mixture of ACN and H_2O. High resolution mass spectra (HRMS) were acquired using a Micromass Q-Tof2 mass spectrometer with electrospray ionization (ESI). HRMS spectra were referenced using a polyethylene glycol polymer mixture, which was co-injected during acquisition as an internal accurate mass standard, unless noted otherwise. Semipreparative HPLC was performed on a Gilson HPLC instrument equipped with a Gilson 215 fraction collector, Agilent PDA detector, and/or ELSD (Sedere) detector. HPLC solvents were obtained from Fisher Scientific and VWR. Deuterated solvents were obtained from Cambridge Isotope Laboratories, Inc. All other chemical reagents were obtained from Sigma-Aldrich.

Synthesis of Compound 6 from 5. Sodium iodide (325 mg, 2.2 mmol) was added to a solution of **5** (78 mg, 0.22 mmol) in acetone and stirred at room temperature for 48 h. The solution was then concentrated under a stream of nitrogen, and this concentrated solution was run on a silica plug in order to remove excess salts. A composition of 25% EtOAc/75% hexanes (25 mL) followed by 50% EtOAc/50% hexanes (4 × 50 mL) was used to elute **6** (74.9 mg, 84%) in the first four fractions.

Total Synthesis of Compound 7. Compound **9** was synthesized as described previously.[28] To a solution of compound **9** (2 mg, 6.78 μmol) in dry CH_2Cl_2 (1 mL) was added Et_3N (9.5 μL, 68 μmol) and tosyl chloride (13 mg, 67.8 μmol), and the solution was stirred at room temperature for 7 h. The reaction progress was monitored by LC−MS. After completion, the reaction mixture was purified on a silica plug to obtain the desired tosylated derivative **10** (2 mg, 4.45 μmol, 66%).

To a solution of **10** (2 mg, 4.45 μmol) in dry CH_2Cl_2 (1 mL) was added Dess−Martin periodinane (4 mg, 9 μmol). The reaction mixture was stirred at room temperature for 4 h and monitored by LC−MS. After completion, the reaction mixture was filtered through a 0.2 μm syringe filter and the filtrate was concentrated to obtain keto derivative **11** (1.5 mg, 3.35 μmol, 75%).

To a solution of **11** (1.5 mg, 3.35 μmol) in isopropyl alcohol (1 mL) and H_2O (10 μL, 1% of the total organic solvent) was added sodium borohydride (0.13 mg, 3.35 μmol). The reaction mixture was stirred at room temperature for 5 min, quenched with 4% aqueous HCl (100 μL), and then extracted with CH_2Cl_2 (2 × 2 mL). The combined organic phase was concentrated under reduced pressure and further purified on silica plug to obtain **7** and its C-5 epimer **10** in 1:1 ratio (1.2 mg, 80%). The two compounds were characterized as a mixture based on mass spectra and HPLC retention times. The mixture was not screened for biological activity. Instead, the pure compound **7** obtained from derivatization of **12** was evaluated.

Synthesis of Compound 7 from 12. To a solution of compound **12** (10 mg, 0.034 mmol) in dry CH_2Cl_2 (2.5 mL) was added Et_3N (47.2 uL, 0.34 mmol) and tosyl chloride (64.8 mg, 0.34 mmol) and stirred at room temperature for 16 h. The reaction mixture was concentrated under reduced pressure, redissolved in 1 mL of ACN, and purified on reversed phase HPLC using an ACE 5 μm C18 column (22 mm × 150 mm) and solvent gradient of 10% ACN, 90% water to 100% ACN over 18 min, holding at 100% ACN for 3 min, at a flow rate of 14.5 mL/min. The purification was monitored by PDA detection. Compound **7** was eluted as a pure compound (5 mg, 32.7%). ESIMS, *m*/*z* 450.3 $[M + H]^+$; HRESIMS *m*/*z* 472.1414 $[M + Na]^+$ (calcd for $C_{22}H_{27}NO_7NaS$, 472.1406);

^{1}H NMR (DMSO-d_6) δ 1.25 (m, 1H), 1.42 (br m, 1H), 1.65 (s, 3H), 1.7 (m, 1H), 1.82 (m, 1H), 1.89 (br m, 2H), 1.91 (br m, 2H), 2.26 (br m, 1H), 2.44 (s, 3H, tosyl), 2.55 (m, 1H), 3.67 (t, J = 8.0 Hz, 1H), 4.31 (t, J = 7.0 Hz, 2H), 5.5 (d, J = 7.0 Hz, C-5(OH)), 5.75 (m, 1H), 5.8 (m, 1H), 7.51 (d, J = 8.0 Hz, 2H, tosyl), 7.82 (d, J = 8.0 Hz, 2H, tosyl), 9.05 (s, NH).

Synthesis of Compound 8 from 12. To a solution of compound **12** (10 mg, 0.034 mmol) in dry CH_2Cl_2 (1.5 mL) was added Et_3N (6.62 uL, 0.048 mmol) and mesyl chloride (3.68 μL, 0.048 mmol). The reaction mixture was stirred at room temperature for 6 h. The reaction mixture was directly concentrated under reduced pressure, redissolved in 1 mL of ACN, and purified using reversed phase HPLC with an ACE 5 μm C18 column (22 mm × 150 mm) and solvent gradient of 10% ACN, 90% water to 100% ACN over 18 min, holding at 100% ACN for 3 min, at a flow rate of 14.5 mL/min. The purification was monitored by PDA detection. Compound **8** was obtained as a pure compound (5 mg, 0.013 mmol, 40%). ESIMS, m/z 374.3 $[M + H]^+$; HRESIMS m/z 396.1111 $[M + Na]^+$ (calcd for $C_{16}H_{23}NO_7NaS$, 396.1093); ^{1}H NMR (DMSO-d_6) δ 1.22 (m, 1H), 1.42 (br m, 1H), 1.73 (m, 1H), 1.76 (s, 3H), 1.85 (m, 1H), 1.94 (br m, 2H), 2.0 (q, J = 7.0 Hz, 2H), 2.31 (br m, 1H), 2.65 (t, J = 6.5 Hz, 1H), 3.22 (s, 3H, SO_2Me), 3.71 (t, J = 8.5 Hz, 1H), 4.48 (t, J = 7.0 Hz, 2H), 5.53 (d, J = 8.0 Hz, C-5(OH)), 5.75 (m, 1H), 5.83 (m, 1H), 9.1 (s, NH).

Synthesis of Compounds 12 and 13 from 6. To a solution of compound **6** (40 mg, 0.099 mmol) in dry THF (4 mL) in the 20 mL amber vial was added AgF (18.8 mg, 0.15 mmol). The reaction mixture was stirred at room temperature for 16 h, then filtered through a 0.45 μm syringe filter and concentrated. The reaction mixture was further purified using reversed phase HPLC with an ACE 5 μm C18 HPLC column of dimensions 22 mm i.d. × 150 mm length at a flow rate of 14.5 mL/min. Solvent A consisted of water with 0.05% trifluoroacetic acid (TFA), and solvent B consisted of ACN with 0.05% TFA. They were used as follows: An initial gradient of 95% solvent A/5% solvent B increased linearly to 60% solvent A/40% solvent B over 18 min; this composition was then held for 8 min followed by a 1 min ramp to 100% solvent B, which was held for 6 min before returning to the initial conditions. The purification was monitored by PDA detection, and **12** eluted at 16 min followed by **13**, which eluted at 21.5 min. Both **12** and **13** were immediately concentrated under reduced pressure (bath temperature of <40 °C) after each injection in order to minimize hydrolysis. Combined fractions containing **13** were subjected to a liquid−liquid extraction of 1:1 EtOAc/water (10 mL), and the resulting organic layer was washed with an additional 5 mL of water to remove polar immunities. A second round of purification using the above method was employed on a sample enriched in **13** followed by a final liquid−liquid extraction as described above in order to remove remaining impurities which yielded **13** (0.1 mg, 0.3%). Compound **12** (11 mg, 15%) was obtained as a pure compound, and spectroscopic data were identical to those of material synthesized by alternative methods.[21]

Compound 13. HRESIMS m/z 298.1455 $[M + H]^+$ (calcd for $C_{15}H_{21}NO_4F$, 298.1455); ESIMS, m/z 298.3 $[M + H]^+$; ^{1}H NMR (DMSO-d_6) δ 1.23 (m, 1H), 1.40 (br m, 1H), 1.69 (m, 1H), 1.73 (s, 3H), 1.82 (m, 1H), 1.92 (br m, 2H), 1.97 (m, 2H), 2.29 (br m, 1H), 2.59 (t, J = 6.9 Hz, 1H), 3.68 (t, J = 8.2 Hz, 1H), 4.67 (m, J = 47.00 Hz, 2H), 5.50 (d, J = 7.9 Hz, C-5(OH)), 5.72 (m, 1H), 5.80 (m, 1H), 9.05 (s, NH).

Synthesis of Compound 16 from 15. Compound **15** (133 mg, 0.425 mmol) was dissolved in dry CH_2Cl_2 (20 mL) and cooled to −78 °C while stirring. DAST was added (280 μL, 2.12 mmol), and the mixture continued to stir at −78 °C. After 35 min, 30 mL of sodium bicarbonate was added to the reaction mixture, which was subsequently extracted with methylene chloride (2 × 30 mL), and the combined organic layers were condensed on the rotary evaporator. This sample was redissolved in 7 mL of acetone and purified using normal phase HPLC (Phenomenex Luna Si 10 μm, 100 Å, 250 mm × 21.2 mm i.d., 750 μL injection volume, flow rate of 25 mL/min) using an isocratic solvent system of 76% hexanes/24% ethyl acetate. Compound **16** eluted as a broad peak between 13 and 15 min. The combined fractions containing **16** were then crystallized in a solvent system of 2:2:1 hexanes/diethyl ether/acetone at room temperature for 20 h. Crystallography data were collected on a Bruker SMART APEX CCD X-ray diffractometer (F(000) = 332, Mo Kα radiation, λ = 0.710 73 Å, μ = 0.282 mm^{-1}, T = 100 K), and the refinement method used was full-matrix least-squares on F^2: molecular formula $C_{15}H_{29}ClFNO_3$, MW = 315.76, monoclinic, space group $P2(1)$, a = 8.861 (5) Å, b = 7.425(4) Å, c = 11.113(6) Å, α = 90°, β = 92.974(9)°, γ = 90°, vol = 730.1(7) Å^3, Z = 2, ρ_{calcd} = 1.436 g cm^{-3}, crystal size = 0.41 × 0.13 × 0.06 mm^3, θ range = 1.83−26.00°, 4611 reflections collected, 2740 independent reflections (R_{int} = 0.0493). Final R indices ($I > 2\sigma(I)$): R1 = 0.0563, wR2 = 0.1339, GOF = 1.016. ESIMS, m/z 298.3 $[M + H]^+$; HRESIMS m/z 298.1461 $[M + H]^+$ (calcd for $C_{15}H_{21}NO_4F$, 298.1455). ^{1}H NMR (DMSO-d_6): δ 1.18 (m, 1H), 1.30−1.45 (m, 4H), 1.50 (t, J = 5 Hz, 1H), 1.51−1.70 (m, 3H), 1.67 (s, 3H), 1.73−1.81 (m, 2H), 2.66 (dd, J = 6, 8.2 Hz, 1H), 3.57 (m, 2H), 5.12 (ddd, J = 52, 12, 6 Hz, 1H), 8.82 (s, NH).

Synthesis of 19 from 12. To a solution of compound **12** (17 mg, 0.058 mmol) in dry CH_2Cl_2 (5 mL) was added Et_3N (36 μL, 0.26 mmol) and dansyl chloride (78.5 mg, 0.29 mmol), and the solution was stirred at room temperature for 24 h. Additional dansyl chloride (78.5 mg, 0.29 mmol) and Et_3N (36 μL, 0.26 mmol) were added, and the mixture was stirred at room temperature overnight. At 42 h, the mixture was concentrated under reduced pressure, redissolved in 5 mL of ACN, and purified on reversed phase HPLC using an ACE 5 μm C18 column (22 mm × 150 mm) at a flow rate of 14.5 mL/min. A solvent gradient of 100% water to 35% ACN/65% water over 8 min, holding at this solvent composition for 2 min, and then a linear gradient increasing to 100% ACN over 5 min, which was then held at 100% ACN for 6 min before returning to 100% water, were used to purify **19**. The purification was monitored by PDA detection, and **19** eluted as a pure compound at 15 min (17 mg, 0.032 mmol, 55.3%). HRESIMS m/z 529.1993 $[M + H]^+$ (calcd for $C_{27}H_{33}N_2O_7S$, 529.2008); ^{1}H NMR (DMSO-d_6) δ 1.18 (br m, 1H), 1.38 (br m, 1H), 1.46 (s, 3H), 1.74 (br m, 4H), 1.90 (m, 2H), 2.19 (m, 1H), 2.42 (t, J = 7.3 Hz 1H), 2.84 (s, 6H, dansyl), 3.60 (t, J = 9.5 Hz, 1H), 4.29 (m, 2H), 5.47 (d, J = 7.9 Hz, C-5(OH)), 5.73 (m, 2H), 7.29 (d, J = 7.6 Hz, 1H, dansyl), 7.67 (m, 2H, dansyl), 8.11 (d, J = 8.8 Hz, 1H, dansyl), 8.26 (dd, J = 1.3, 7.3 Hz, 1H, dansyl), 8.59 (d, J = 8.8 Hz, 1H, dansyl), 8.99 (s, NH).

Analogue Stability in Proteasome Assay Buffer. Stability of the compounds was monitored in proteasome assay buffer (20 mM HEPES, 0.5 mM EDTA, and 0.05% Triton X-100, pH 7.3) at 37 °C. The buffer solution was pre-equilibrated at 37 °C for 30 min on the HPLC autosampler (Agilent 1100). Compounds were prepared as 1 mg/mL stock solutions in ACN, and aliquots (50 μL) were spiked into pre-equilibrated buffer (950 μL) to a final concentration of 50 μg/mL. The solutions were analyzed over time by sequential injection of 25 μL aliquots onto an Agilent analytical HPLC 1100 MSD system equipped with a PDA detector and a C-18 column (ACE 3 μm C18, 150 mm × 4.6 mm, column temperature 30 °C). The concentrations of compounds **19** (25 μg/mL with the injection volume of 15 μL) and **7** (25 μg/mL with the injection volume of 25 μL) were different because of the high UV absorbance; however, the rate of β-lactone hydrolysis of **1** has been established as following first-order kinetics.[34] Thus, $T_{1/2}$ values are concentration-independent. The HPLC mobile phases were as follows: A, 0.01% aqueous TFA; B, 0.01% TFA in ACN. The gradient commenced with 100% A (1 min) followed by linear increase to 100% B over the next 15 min at a flow rate of 1 mL/min. HPLC autosampler temperature was monitored periodically with an external temperature probe. The starting materials were identified by their established HPLC retention times and confirmed by mass spectrometry, and hydrolysis products were identified by mass spectrometry. $T_{1/2}$ values for disappearance of starting material were determined from the time at which the UV peak area percent (mAU•s) of the starting material was 50% that of its UV peak area percent at time zero. Compound **1** was used as a reference standard by repeating the hydrolysis experiment three times, once at the

beginning of the sequence of analogues and subsequently interleaved between analogues analyzed later in the sequence. Hydrolysis of **1** was performed twice at 50 μg/mL and once at 25 μg/mL; the $T_{1/2}$ mean and standard deviation for the three experiments are reported.

In Vitro Purified Yeast 20S Proteasome Activity Assays. Yeast 20S proteasome was purified as described previously,[53] and the determination of all three yeast 20S proteolytic activities was modified from the method described by Kimura et al.[54] The CT-L activity was determined by adding serial diluted compounds to purified yeast 20S proteasome in assay buffer containing 75 mM Tris-HCl, pH7.8, and 0.02% SDS and preincubated for 5 min at 37 °C. Reactions were initiated by the addition of the Suc-LLVY-AMC peptide substrate at a final concentration of 20 μM. Fluorescence of the cleaved AMC (7-amino-4-methylcoumarin) was measured at $\lambda_{ex} = 390$ nm and $\lambda_{em} = 460$ nm using a Fluoroskan Ascent 96-well microplate reader (Thermo Electron). The IC_{50} values (the drug concentration at which 50% of the maximal relative fluorescence is inhibited) were calculated by Prism (GraphPad Software) using a sigmodial dose−response, variable slope model. The C-L activity of the yeast 20S proteasome was determined as described above except that Z-LLE-AMC was used as substrate. For the evaluation of the T-L activity, the SDS was omitted from the assay buffer and Bz-VGR-AMC was used as peptide substrate.

In Vitro Purified Rabbit Muscle 20S Proteasome Activity Assays. The determination of all three rabbit 20S proteolytic activities[55] was essentially the same as described above with the following modifications. The CT-L and C-L activities were determined in 20 mM HEPES, pH 7.3, 0.05% Triton X-100, 0.5 mM EDTA, and 0.035% SDS assay buffer using the same peptide substrates as described in the previous section. For the evaluation of the T-L activity, SDS was omitted from the buffer and the Boc-LRR-AMC peptide was used as substrate. The final concentration of purified rabbit 20S proteasome was 1.4 nM.

Dialysis Using Purified Rabbit 20S Proteasomes. A Spectra/Por 10-well MicroDialyzer (Spectrum Laboratories) was assembled according to the manufacturer's instructions using Spectra/Por MWCO 12−14000 membranes. Compounds or DMSO were added to rabbit 20S proteasomes (Boston Biochem) and incubated for 1 h at ambient temperature in proteasome assay buffer (20 mM HEPES, 0.5 mM EDTA, 0.05% Triton X-100, 0.035% SDS, pH 7.3) at a final 20S proteasome concentration of 1.4 nM and 0.1% DMSO. (SDS is omitted from the proteasome assay buffer for determination of T-L 20S proteasome activity, as noted above.) Compounds were evaluated at concentrations that corresponded to their IC_{50} values determined for the in vitro inhibition of rabbit 20S CT-L, T-L, or C-L proteasome activity.

After the 1 h of incubation, proteasome−compound mixtures were added to the wells of the MicroDialyzer and dialyzed against proteasome assay buffer. Immediately ($t = 0$) and after 1, 2, 5, and 24 h of dialysis at ambient temperature, samples were removed from single wells and the CT-L, T-L, or C-L 20S proteasome activity was determined. Compounds **4**, **12**, **13**, **20**, and **21** were also evaluated after 12 h of dialysis, and compound **1** was evaluated after 18 h of dialysis. Proteasome activity was normalized against proteasome activity of DMSO controls.

Dialysis Using Human 20S Proteasomes. All three proteolytic activities of the 20S proteasome were completely inhibited by preincubating 50 nM enzyme with 1 μM inhibitor **1** in 20 mM HEPES (pH 8.0), 0.5 mM EDTA, and 0.035% SDS for 20 min, with inhibition confirmed via enzymatic activity assays. Reversibility was ascertained by dialyzing 700 μL of the 20S proteasome−inhibitor complex against 1 L of chymotrypsin reaction buffer for 12 h. To ensure no loss of enzymatic activity during the dialysis process, an analogous 20S-proteasome dialysis in the absence of inhibitor was performed. After dialysis of the inhibitor−20S-proteasome complex, potential recovery of enzymatic activity was assayed using 200 μM of the respective substrate. T-L site activity was assayed at 1 nM 20S proteasome, and CT-L and C-L activity were assayed at 0.25 nM proteasome, as described above.

Enzyme Inhibition Kinetics for 1 with Human 20S Proteasomes. Reagents and Buffers. All chemicals were of reagent grade. Buffers were made with deionized distilled H_20. Buffer A (20 mM HEPES (pH 8.0), 0.5 mM EDTA, and 0.035% SDS) was used for the CT-L and C-L activity assays. Buffer B (20 mM HEPES (pH 8.0) and 0.5 mM EDTA) was used for the T-L activity assays. Human 20S proteasomes were purchased from Biomol (catalog no. 8720) at a stock concentration of 3.5 μM. All AMC peptide substrates were purchased from Bachem and made to 50 mM stock concentrations in DMSO. Suc-LLVY-AMC, boc-LRR-AMC, and Z-LLE-AMC were used to monitor the CT-L, T-L, and C-L activities, respectively. Stock solutions of **1** (32 mM) were made up in DMSO.

Equipment Setup. All inhibition experiments were performed using a PTI (Photon Technology Instrument) Quantmaster fluorimeter. Excitation and emission wavelengths were set to 380 and 440 nm, respectively, with a 5 nm bandpass. All experiments were performed at 37 °C in 3 mL quartz cuvettes with the temperature maintained via a jacketed four-turrett cuvette holder and controlled via a refrigerated water bath.

The enzymatic assay monitors the release of AMC from the respective substrates, resulting in an increase in fluorescence. Site specific inhibition mechanism studies were performed at 2 μM substrate and varying concentrations of **1**. The reactions were initiated by the addition of 20S proteasome to a final concentration of 1 nM for the T-L activity and 0.25 nM for the CT-L and C-L activity. The reaction was monitored in a continuous kinetic manner over 30 min. K_m values determined for each of the enzymatic activities were 36, 22, and 24 μM for the CT-L, T-L, and C-L sites, respectively. The substrate concentration used in the inhibition experiments were therefore significantly below the K_m for each of the sites. AMC calibration curves were linear over the range of AMC produced by the respective enzymatic reactions.

Acknowledgment. We thank A. Rheingold, University of California, San Diego, for determining the X-ray crystal structure of **16**; G. Deyanat-Yazdi for measuring IC_{50} values for the inhibition of yeast 20S proteasomes by **1** and **4**; and V. Stella, University of Kansas, for helpful discussions regarding analogue hydrolysis.

Supporting Information Available: Purity of compounds and methods of determination thereof. This material is available free of charge via the Internet at http://pubs.acs.org.

References

(1) Orlowski, R. Z.; Kuhn, D. J. Proteasome Inhibitors in Cancer Therapy: Lessons from the First Decade. *Clin. Cancer Res.* **2008**, *14*, 1649–1657.
(2) Adams, J. *Proteasome Inhibitors in Cancer Therapy*; Humana Press: Totowa, NJ, 2004.
(3) Kisselev, A. F.; Goldberg, A. L. Proteasome Inhibitors: From Research Tools to Drug Candidates. *Chem. Biol.* **2001**, *8*, 739–758.
(4) Hershko, A.; Ciechanover, A. The Ubiquitin System. *Annu. Rev. Biochem.* **1998**, *67*, 425–479.
(5) Borissenko, L.; Groll, M. 20S Proteasome and Its Inhibitors: Crystallographic Knowledge for Drug Development. *Chem. Rev.* **2007**, *107*, 687–717.
(6) Groll, M.; Bochtler, M.; Brandstetter, H.; Clausen, T.; Huber, R. Molecular Machines for Protein Degradation. *ChemBioChem* **2005**, *6*, 222–256.
(7) Groll, M.; Huber, R. Inhibitors of the Eukaryotic 20S Proteasome Core Particle: A Structural Approach. *Biochim. Biophys. Acta* **2004**, *1695*, 33–44.
(8) Groll, M.; Ditzel, L.; Löwe, J.; Stock, D.; Bochtler, M.; Bartunik, H. D.; Huber, R. Structure of 20S Proteasome from Yeast at 2.4 Å Resolution. *Nature* **1997**, *386*, 463–471.
(9) Löwe, J.; Stock, D.; Jap, B.; Zwickl, P.; Baumeister, W.; Huber, R. Crystal Structure of the 20S Proteasome from the Archaeon *T. Acidophilum* at 2.4 Resolution. *Science* **1995**, *268*, 533–539.
(10) Wilk, S.; Pereira, M.; Yu, B. Probing the Specificity of the Bovine Pituitary Multicatalytic Proteinase Complex by Inhibitors, Activators, and by Chemical Modification. *Biomed. Biochim. Acta* **1991**, *50*, 471–478.

(11) Kisselev, A. F.; Callard, A.; Goldberg, A. L. Importance of the Different Proteolytic Activities of the Proteasome and the Efficacy of the Inhibitors Varies with the Protein Substrate. *J. Biol. Chem.* **2006**, *281*, 8582–8590.

(12) Bross, P. F.; Kane, R.; Farrell, A. T.; Abraham, S.; Benson, K.; Brower, M. E.; Bradley, S.; Gobburu, J. V.; Goheer, A.; Lee, S.-L.; Leighton, J.; Liang, C. Y.; Lostritto, R. T.; McGuinn, W. D.; Morse, D. E.; Rahman, A.; Rosario, L. A.; Verbois, S. L.; Williams, G.; Wang, Y.-C.; Pazdur, R. Approval Summary for Bortezomib for Injection in the Treatment of Multiple Myeloma. *Clin. Cancer Res.* **2004**, *10*, 3954–3964.

(13) Richarson, P. G.; Barlogie, B.; Berenson, J.; Singhal, S.; Jagannath, S.; Irwin, D.; Rajkumar, S. V.; Srkalovic, G.; Alsina, M.; Alexanian, R.; Seigel, D.; Orlowski, R. Z.; Kuter, D.; Limentani, S. A.; Lee, S.; Hideshima, T.; Esseltine, D. L.; Kauffman, M.; Adams, J.; Schenkein, D. P.; Anderson, K. C. A Phase 2 Study of Bortezomib in Relapsed, Refractory Myeloma. *N. Engl. J. Med.* **2003**, *348*, 2609–2617.

(14) Suh, K. S.; Goy, A. Bortezomib in Mantle Cell Lymphoma. *Future Oncol.* **2008**, *4*, 149–168.

(15) Feling, R. H.; Buchanan, G. O.; Mincer, T. J.; Kauffman, C. A.; Jensen, P. R.; Fenical, W. Salinosporamide A: A Highly Cytotoxic Proteasome Inhibitor from a Novel Microbial Source, a Marine Bacterium of the New Genus *Salinospora*. *Angew.Chem. Int. Ed.* **2003**, *42*, 355–357.

(16) Omura, S.; Matsuzaki, K.; Fujimoto, T.; Kosuge, K.; Furuya, T.; Fujita, S.; Nakagawa, A. Structure of Lactacystin, a New Microbial Metabolite Which Induces Differentation of Neuroblastoma Cells. *J. Antibiot.* **1991**, *44*, 117–118.

(17) Corey, E. J.; Li, W. Z. Total Synthesis and Biological Activity of Lactacystin, Omuralide, and Analogs. *Chem. Pharm. Bull.* **1999**, *47*, 1–10.

(18) Dick, L. R.; Cruikshank, A. A.; Grenier, L.; Melandri, F. D.; Nunes, S. L.; Stein, R. L. Mechanistic Studies on the Inactivation of the Proteasome by Lactacystin. *J. Biol. Chem.* **1996**, *271*, 7273–7276.

(19) Shah, I. M.; Lees, K. R.; Pien, C. P.; Elliot, P. J. Early Clinical Experience with the Novel Proteasome Inhibitor PS-519. *Br. J. Clin. Pharmacol.* **2002**, *54*, 269–276.

(20) Williams, P. G.; Buchanan, G. O.; Feling, R. H.; Kauffman, C. A.; Jensen, P. R.; Fenical, W. New Cytotoxic Salinosporamides from the Marine Actinomycete *Salinispora tropica*. *J. Org. Chem.* **2005**, *70*, 6196–6203.

(21) Macherla, V. R.; Mitchell, S. S.; Manam, R. R.; Reed, K.; Chao, T.-H.; Nicholson, B.; Deyanat-Yazdi, G.; Mai, B.; Jensen, P. R.; Fenical, W.; Neuteboom, S. T. C.; Lam, K. S.; Palladino, M. A.; Potts, B. C. M. Structure−Activity Relationship Studies of Salinosporamide A (NPI-0052), a Novel Marine Derived Proteasome Inhibitor. *J. Med. Chem.* **2005**, *48*, 3684–3687.

(22) Reed, K. A.; Manam, R. R.; Mitchell, S. S.; Xu, J.; Teisan, S.; Chao, T.-H.; Deyanat-Yazdi, G.; Neuteboom, S. T. C.; Lam, K. S.; Potts, B. C. M. Salinosporamides D-J from the Marine Actinomycete *Salinispora tropica*, Bromosalinosporamide, and Thioester Derivatives Are Potent Inhibitors of the 20S Proteasome. *J. Nat. Prod.* **2007**, *70*, 269–276.

(23) Chauhan, D.; Catley, L.; Li, G.; Podar, K.; Hideshima, T.; Velankar, M.; Mitsiades, C.; Mitsiades, N.; Yasui, H.; Letai, A.; Ovaa, H.; Berkers, C.; Nicholson, B.; Chao, T.-H.; Neuteboom, S. T. C.; Richardson, P.; Palladino, M.; Anderson, K. C. A Novel Orally Active Proteasome Inhibitor Induces Apoptosis in Multiple Myeloma Cells with Mechanisms Distinct from Bortesomib. *Cancer Cell* **2005**, *8*, 407–419.

(24) Cusack, J. C., Jr.; Liu, R.; Xia, L.; Chao, T.-H.; Pien, C.; Niu, W.; Palombella, V. J.; Neuteboom, S. T.; Palladino, M. A. NPI-0052 Enhances Tumoricidal Response to Conventional Cancer Therapy in a Colon Cancer Model. *Clin. Cancer Res.* **2006**, *12*, 6758–6764.

(25) Ruiz, S.; Krupnik, Y.; Keating, M.; Chandra, J.; Palladino, M.; McConkey, D. The Proteasome Inhibitor NPI-0052 Is a More Effective Inducer of Apoptosis Than Bortezomib in Lymphocytes from Patients with Chronic Lymphocytic Leukemia (CLL). *Mol. Cancer Ther.* **2006**, *5*, 1836–1843.

(26) Groll, M.; Huber, R.; Potts, B. C. M. Crystal Structure of Salinosporamide A (NPI-0052) and B (NPI-0047) in Complex with the 20S Protesome Reveal Important Consequences of β-Lactone Ring Opening and a Mechanism for Irreversible Binding. *J. Am. Chem. Soc.* **2006**, *128*, 5136–5141.

(27) Fenteany, G.; Standaert, R. F.; Lane, W. S.; Choi, S.; Corey, E. J.; Schreiber, S. L. Inhibition of Proteasome Activities and Subunit-Specific Amino-Terminal Threonine Modification by Lactacystin. *Science* **1995**, *268*, 726–731.

(28) Ling, T.; Macherla, V. R.; Manam, R. R.; McArthur, K. A.; Potts, B. C. M. Enantioselective Total Synthesis of (−)-Salinosporamide A (NPI-0052). *Org. Lett.* **2007**, *9*, 2289–2292.

(29) Lam, K. S.; Tsueng, G.; McArthur, K. A.; Mitchell, S. S.; Potts, B. C. M. Effects of Halogens on the Production of Salinosporamides by the Obligate Marine Actinomycete *Salinispora tropica*. *J. Antibiot.* **2007**, *60*, 13–19.

(30) Reddy, L. R.; Reddy, B. V. S.; Corey, E. J. Efficient Method for Selective Introduction of Substituents as C(5) of Isoleucine and Other α-Amino Acids. *Org. Lett.* **2006**, *8*, 2819–2821.

(31) Moody, C. J.; Hunt, P. A.; Smith, C. Iodocyclisation of *N*-Allyl Ureas; A Route to Imidazolin-2-ones. *ARKIVOC* **2000**, (v), 698–706.

(32) We hypothesized that the DAST was reacting with secondary alcohol (C-5) and then undergoing either nucleophilic addition to the cyclohexene ring (C-5 (*R*)) or degradation (C-5 (*S*)). Thus, various protecting group strategies (e.g., TMS, TES, or oxidation) were used on **6** and **12** to obtain the C-5OH protected derivative of **12**, but in all cases, either a degradant formed or deprotection occurred when DAST or AgF was used. We did not target the total synthesis of a C-5OH-protected derivative of **9**.

(33) Suenaga, T.; Schutz, C.; Nakata, T. A Real Time Reaction Monitoring Using Fluorescent Dansyl Group as a Solid-Phase Leaving Group. *Tetrahedron Lett.* **2003**, *44*, 5799–5801.

(34) Denora, N.; Potts, B. C. M.; Stella, V. J. A Mechanistic and Kinetic Study of the β-lactone Hydrolysis of Salinosporamide A (NPI-0052), a Novel Proteasome Inhibitor. *J. Pharm. Sci.* **2007**, *96*, 2037–2047.

(35) Djuric, S. W.; Garland, R. B.; Nysted, L. N.; Pappo, R.; Plume, G.; Swenton, L. Sythesis of 5-Fluoroprostacyclin. *J. Org. Chem.* **1987**, *52*, 978–990.

(36) Toscano, L.; Fioriello, G.; Silingardi, S.; Inglesi, M. Preparation of (8*S*)-8-Fluoroerythronolide A and (8*S*)-8-Fluoroerythronolide B, Potential Substrates for the Biological Synthesis of New Macrolide Antibiotics. *Tetrahedron* **1984**, *40*, 2177–2181.

(37) Stadler, M.; Bitzer, J.; Mayer-Bartschmid, A.; Muller, H.; Benet-Buchholz, J.; Gantner, F.; Tichy, H.-V.; Reinemer, P.; Bacon, K. B. Cinnabaramides A−G: Analogs of Lactacystin and Salinosporamide from a Terrestrial Streptomycete. *J. Nat. Prod.* **2007**, *70*, 246–252.

(38) It is conceivable that the "irreversible inhibition" by LG analogues could be the result of a stable covalent bond between the inhibitor and the proteasome borne from direct alkylation via the chlorethyl group (as an alternative to or in addition to the covalent ester bond to Thr1Oγ). However, there was *no evidence of any direct alkylation product in the crystal structure of* **1** with the 20S proteasome; only the *intramolecular* chloride displacement product (cyclic ether end product **Ib′**) was observed.[26] Thus, there is little evidence to support the hypothesis that the longer duration of proteasome inhibition in the case of **1** (or other analogues in the LG family) results from direct alkylation of proteasome amino acid(s) by the chloroethyl group. Moreover, direct reactions of **1** or closely related compounds with nucleophiles that may mimic amino acid side chains, including primary alcohols, water or hydroxide, thiols, and amines, have resulted in minimal or no direct displacement of chloride. Reaction of **1** with nucleophiles, hydroxide or water,[21] MeOH,[20] and thiol[22] initially cleaved the β-lactone ring and produced carboxylic acid, methylester and thioesters, respectively, which were further converted to form the corresponding cyclic ether ring product by intramolecular displacement of chloride with C-3 OH with no report on direct displacement of chloride with those of nucleophiles used in the reaction. Reaction of a synthetic analogue of **1** with primary amine (benzylamine) also produced similar products with no report on direct replacement of chloride.[39] In one instance, trace amounts (2%) of the disubstituted product of β-lactone cleavage and chloride displacement were detected in the reaction mixture by LC−MS when compound **1** was reacted with benzene thiol. Reaction of **1** with triethylamine at 40 °C (our own findings) or NaOH[20] gave decarboxylation (by β-elimination of carboxylate) products with no reports on displacement of chloride. Reaction of iodosalinosporamide (**6**) with NaOH gave **12** as a minor byproduct;[21] we note that **6** is a better substrate for halogen displacement than **1**.

(39) Reddy, L. R.; Fournier, J.-F.; Reddy, B. V. S.; Corey, E. J. An Efficient, Stereocontrolled Synthesis of a Potent Omuralide−Salinosporin Hybrid for Selective Proteasome Inhibition. *J. Am. Chem. Soc.* **2005**, *127*, 8974–8976.

(40) Morrison, J. F.; Walsh, C. T. The Behavior and Significance of Slow-Binding Inhibitors. *Adv. Enzymol.* **1988**, *61*, 201–301.

(41) Jaramillo, P.; Domingo, L. R.; Perez, P. Towards an Intrinsic Nucleofugality Scale: The Leaving group (LG) Ability in CH_3LG Model System. *Chem. Phys. Lett.* **2006**, *420*, 95–99.

(42) The β-lactone hydrolysis product of **4** did not inhibit the CT-L, T-L, or C-L activities of rabbit 20S proteasomes at the highest concentrations tested (IC_{50} > 20 μM; unpublished result).

(43) Eustaquio, A. S.; Moore, B. S. Mutasynthesis of Fluorosalinosporamide, a Potent and Reversible Inhibitor of a Proteasome. *Angew. Chem., Int. Ed.* **2008**, *47*, 3936−3938.

(44) O'Hagan, D.; Rzepa, H. S. Some Influences of Fluorine in Bioorganic Chemistry. *Chem. Commun.* **1997**, 645–652.

(45) Olsen, J. A.; Banner, D. W.; Seiler, P.; Wagner, B.; Tschopp, T.; Obst-Sander, U.; Kansy, M.; Muller, K.; Diederich, F. Fluorine Interactions

at the Thrombin Active Site: Protein Backbone Fragments H−Cα−C═O Comprise a Favorable C−F Environment and Interactions of C−F Electrophiles. *ChemBioChem* **2004**, *5*, 666–675.
(46) Bohm, H.-J.; Banner, D.; Bendels, S.; Kansy, M.; Kuhn, B.; Muller, K.; Obst-Sander, U.; Stahl, M. Fluorine in Medicinal Chemistry. *ChemBioChem* **2004**, *5*, 637–643.
(47) Biffinger, J. C.; Kim, H. W.; DiMagno, S. G. The Polar Hydrophobicity of Fluorinated Compounds. *ChemBioChem* **2004**, *5*, 622–627.
(48) Howard, J. A. K.; Hoy, V. J.; O'Hagen, D.; Smith, G. T. How Good Is Fluorine As a Hydrogen Bond Acceptor? *Tetrahedron* **1996**, *38*, 12613–12622.
(49) Dunitz, J. D.; Taylor, R. Organic Fluorine Hardly Ever Accepts Hydrogen Bonds. *Chem.—Eur. J.* **1997**, *3*, 89–98.
(50) Carosati, E.; Sciabola, S.; Cruciani, G. Hydrogen Bonding Interactions of Covalently Bonded Fluorine Atoms: From Crystallographic Data to a New Angular Function in the GRID Force Field. *J. Med. Chem.* **2004**, *47*, 5114–5125.
(51) Seebach, D. Organic Synthesis—Where Now? *Angew. Chem., Int. Ed. Engl.* **1990**, *29*, 1320–1367.
(52) Chao, T. C.; Barral, A. M.; Lloyd, G. K.; Spear, M.; Palladino, M. A.; Neuteboom, S. T. The Pharmacodynamic Profile of NPI-0052 Is Cell-Type Specific. *Proceedings of the 101st Annual Meeting of the American Association for Cancer Research*, San Diego, California, April 12−16, 2008; AACR: Philadelphia, PA, 2008; Abstract 3257, p 773.
(53) Groll, M.; Huber, R. Purification, Crystallization and X-ray Analysis of the Yeast 20S Proteasomes. *Methods Enzymol.* **2005**, *398*, 329–336.
(54) Kimura, Y.; Takaoka, M.; Tanaka, S.; Sassa, H.; Tanaka, K.; Polevoda, B.; Sherman, F.; Hirano, H. N^{α}-Acetylation and Proteolytic Activity of the Yeast 20S Proteasome. *J. Biol. Chem.* **2000**, *275*, 4635–4639.
(55) Stein, R. L.; Melandri, F.; Dick, L. Kinetic Characterization of the Chymotryptic Activity of the 20S Proteasome. *Biochemistry* **1996**, *35*, 3899–3908.

JM800548B